Post-Synthetic Covalent and Coordination Functionalization of Rhodium(II)-based Metal-Organic Polyhedra

Arnau Carné-Sánchez,[†,#,*] Jorge Albalad,[†,#] Thais Grancha,[†,#] Inhar Imaz,[†] Judith Juanhuix,[‖] Patrick Larpent,[⊥] Shuhei Furukawa[⊥,§,*] and Daniel Maspoch[†, ‡,*]

[†] Catalan Institute of Nanoscience and Nanotechnology (ICN2), CSIC and The Barcelona Institute of Science and Technology, Campus UAB, Bellaterra, 08193 Barcelona, Spain

[‖]ALBA Synchrotron, 08290 Cerdanyola del Vallès, Barcelona, Spain

[⊥]Institute for Integrated Cell-Material Science (WPI-iCeMS), Kyoto University, Yoshida, Sakyo-ku, Kyoto 606-8501, Japan

[§]Department of Synthetic Chemistry and Biological Chemistry, Graduate School of Engineering, Kyoto University, Katsura, Nishikyo-ku, Kyoto 615-8510, Japan

[‡] ICREA, Pg. Lluís Companys 23, 08010 Barcelona, Spain

ABSTRACT: Metal-organic polyhedra (MOPs) are ultra-small (typically 1 nm to 4 nm) porous coordination cages made from the self-assembly of metal ions and organic linkers and amenable to the chemical functionalization of its periphery; however, it has been challenging to implement post-synthetic functionalization due to their chemical instability. Herein, we report the use of coordination chemistries and covalent chemistries to post-synthetically functionalize the external surface of ≈2.5 nm stable Rh(II)-based cuboctahedra through their Rh-Rh paddlewheel units or organic linkers, respectively. We demonstrate that 12 N-donor ligands, including amino acids, can be coordinated on the periphery of Rh-MOPs. We used this reactivity to introduce new functionalities (*e.g.* chirality) to the MOPs and to tune their hydrophilicity/hydrophobic character, which allowed us to modulate their solubility in diverse solvents such as dichloromethane and water. We also demonstrate that all 24 organic linkers can be post-synthetically functionalized with esters via covalent chemistry. In addition, we anticipate that these two types of post-synthetic reactions can be combined to yield doubly-functionalized Rh-MOPs, in which a total of 36 new functional molecules can be incorporated on their surfaces. Likewise, these chemistries could be synergistically combined to enable covalent functionalization of MOPs through new linkages such as ethers. We believe that both reported post-synthetic pathways can potentially be used to engineer Rh-MOPs as scaffolds for applications in delivery, sorption and catalysis.

INTRODUCTION

Ultra-small inorganic nanoparticles are important because they fill the gap between the molecular and the nanoscale regimes.[1] On this scale, nanoparticles can merge properties of both regimes, such as solubility in different media with high reactivity and unique physicochemical and pharmacokinetic properties.[2-6] Constructed from the self-assembly of metal ions and organic linkers, metal-organic polyhedra (MOPs) fall into this size scale[7] and, as a subclass of molecular cages[8-11] that can host molecules in solution, they are permanently porous in the solid state.[12-16] An archetypical MOP is the cuboctahedron [M2(m-bdc)2]12 (where M = Cu(II), Cr(II), Mo(II), Rh(II), Ru(II) or even heterometallic; and m-bdc = 1,3-benzenedicarboxylate], which is □2.5 nm in size.[17] It is assembled from 12 M(II)-M(II) paddle-wheel units connected through 24 m-bdc linkers, and has an internal cavity of 1.9 nm that is accessible from eight triangular apertures of 8 Å and six square apertures of 12 Å.

Practical applications of ultra-small inorganic nanoparticles demand chemical functionalization of their external surface,[18] as it enables their stabilization and protection, tuning of their hydrophilic/hydrophobic character, and introduction of new functional molecules in to them (e.g. to modulate interactions between the nanoparticles and Biosystems).[19,20] The latter case is essential for biomedical applications of nanoparticles.[21]

As ultra-small inorganic nanoparticles and MOPs are similarly sized, we reasoned that post-synthetic chemical functionalization of the external surface of MOPs should analogously be crucial for tuning their own properties (e.g. solubility, porosity, etc.) and behavior in various solution-phase (e.g. delivery systems, adsorbents, catalysis) or solid-state (e.g. gas sorption) applications, as well as defining their solubility in diverse solvents. However, to date, post-synthetic functionalization of MOPs has been limited to reactions run under soft conditions,[22] such as click chemistry based on strain-promoted azide-alkyne cycloaddition,[23] synthesis of secondary amines or amides from amino-functionalized MOPs[24-26], or polymerizations based on reverse addition-fragmentation transfer (RAFT) on MOPs functionalized with dithiobenzoate trithioester groups.[27] This is mainly due to the use of chemically unstable MOPs made of highly labile Cu(II) – carboxylate coordination bonds.

Herein we report spatially and stoichiometrically controlled post-synthetic functionalization of MOPs via two different sites-specific chemistries: coordination chemistry on the metal ions and covalent chemistry on the organic linkers. We selected two

robust cuboctahedral Rh(II)-based MOPs: [Rh2(bdc)2(H2O)2]12 (hereafter named as HRhMOP) and [Rh2(OH-bdc)2(H2O)1(DMA)1]12 (hereafter named as OHRhMOP; where OH-bdc = 5-hydroxy-1,3-benzenedicarboxylate and DMA = N,N-dimethylacetamide) (Figure 1a). We chose them for their high microporosity (the BET surface area [SBET] of HRhMOP is 947 m^2/g and that of Rh-OH-MOP, 548 m^2/g) and for their chemical robustness, as they can withstand aggressive reaction conditions, including high temperatures and the presence of strong bases and/or coordinating molecules. Moreover, these MOPs have two distinct reaction sites (Figure 1b): their 12 Rh-Rh paddlewheels, each of which has an exohedral axial site that can undergo ligand-exchange reactions; and their 24 organic ligands, which can bear exohedral reactive functional groups (in this case, hydroxyl groups) to enable functionalization of the metal-organic cuboctahedron via covalent chemistry. We have demonstrated spatial control of these modifications by functionalizing both HRhMOP and OHRhMOP with different N-donor ligands and by using the hydroxyl groups of the OHRhMOP as nucleophiles for synthesis of esters and ethers. Finally, we have determined that these two chemistries can be run sequentially or even simultaneously on a single MOP to yield multivariate Rh-MOPs functionalized with a total of 36 molecules/groups (Figure 1b). With this approach, we demonstrated that chemical transformations can be performed on a nanoscale object while preserving all the distinctive features of molecular chemistry, such as the presence of well-defined reactive sites that can be reacted stoichiometrically and characterized at the molecular level by spectroscopic and crystallographic techniques.

RESULTS AND DISCUSSION

Post-synthetic functionalization via coordination chemistry

Isolated Rh-Rh paddlewheel clusters are inert at their equatorial sites but are highly reactive at their axial sites. For instance, they show high affinity towards N-donor ligands,[28] and their reactions with said ligands can be monitored by following the spectroscopic changes of the band centered at 500 nm to 600 nm, which corresponds to the $\pi^* \rightarrow \sigma^*$ transitions (λ_{max}) of Rh-Rh bonds.[29] Given this affinity, we envisaged that ligand-exchange reactions at these axial sites would enable functionalization of the surface of Rh-MOPs that contain 12 N-donor ligands. Thus, we selected three chemically distinct N-donor ligands (Figure 2a): 4-*tert*-butylpyridine (tertPy); 4-trifluoromethyl pyridine (CF_3-Py), as a source of hydrophobicity; and L-proline (L-Prol), to make the Rh-MOPs more biocompatible and to confer them with chirality and hydrophilicity.

We first tested functionalization of Rh-MOPs via coordination chemistry by adding tertPy (12 mol. eq. [i.e. one per Rh-Rh paddlewheel]) to HRhMOP in DMF at room temperature (Figure 2a). Addition of tertPy led to immediate dissolution of the MOP, as indicated by a concomitant color change from colorless to purple, which is characteristic of the nitrogen coordination to the Rh-Rh paddlewheel clusters (Figure 2a). This was a first indication that ligand exchange between the tertPy ligands and water molecules had occurred. Thus, we attributed the solubility of the resultant MOP in DMF to the bulky *tert*-butyl groups incorporated onto the surface of HRhMOP, as they would inhibit its aggregation and enable DMF molecules to solvate it.

Remarkably, purple crystals suitable for single crystal X-ray diffraction analysis (SCXRD) were obtained by exposing the purple solution to diethyl ether vapors for 5 days. SCXRD analysis (performed on the XALOC beamline of the ALBA synchrotron[30]) confirmed functionalization of the outer surface of HRhMOP with 12 tertPy ligands (Figure 3a). As expected, these tertPy ligands were coordinated to the outer axial site of all Rh-Rh paddle-wheel units, affording a functionalized Rh-MOP of formula $[Rh_2(bdc)_2(tertPy)_1(H_2O)_1]_{12}$ (hereafter referred to as *HRhMOP(tertPy)*).

Having confirmed the functionalization of the outer surface of HRhMOP via SCXRD, we then established a methodology to follow the ligand exchange, based on UV-Vis and ^{1}H-NMR spectroscopies (Figures 2b, 2c, S3 and S4). To this end, $[Rh_2(Ac)_4]$ (where Ac is acetate) was used as a model Rh-Rh paddlewheel cluster to first monitor the spectroscopic changes in the UV-VIS spectra caused by the coordination of tertPy to it. We found that, upon addition of tertPy to a DMF solution of $[Rh_2(Ac)_4]$, λ_{max} shifted from 585 nm to 555 nm, as the ligand bound to one of the available axial sites. Coordination to the second available axial site induced a further shift of λ_{max}, to 538 nm (Figure S3). Interestingly, the UV-VIS spectrum of HRhMOP (tertPy) showed a λ_{max} of 555 nm, matching with the coordination of one tertPy ligand to each of the 12 Rh-Rh paddlewheel units (Figure 2b). Further addition of tertPy to HRhMOP(tertPy) did not cause any additional shift in the λ_{max}, thereby confirming that tertPy can only coordinate to the outer part of HRhMOP. Moreover, ^{1}H-NMR spectra of HRhMOP(tertPy) evidenced coordinated tertPy, as indicated by two aromatic peaks (at 9.52 ppm and 8.66 ppm) corresponding to the pyridine moiety and a peak at 1.54 ppm corresponding to the *tert*-butyl groups (Figure 2c). Finally, we determined the amount of coordinated tertPy ligands by comparing integration of the peaks of the tertPy with the peaks ascribed to the bdc ligand of the HRhMOP (8.10 ppm, 7.87 ppm and 7.18 ppm) (Figure S4). As expected, the molar ratio of tertPy ligands to HRhMOP was 12:1.

We then used the two aforementioned techniques to follow the coordination-induced functionalization of OHRhMOP with tertPy. The reaction was done analogously to HRhMOP, and similarly yielded a purple solution upon addition of tertPy to a DMF suspension of OHRhMOP. Synthesis of the expected MOP $[Rh_2(OH\text{-}bdc)_2(tertPy)_1(H_2O)_1]_{12}$ was confirmed by UV-Vis (λ_{max} = 555 nm; Figure S5) and ^{1}H-NMR (Figure S6).

Once we had demonstrated that the surface of Rh-based MOPs can be selectively functionalized via coordination chemistry, and that such reactions yield products whose solubility profile differs from that of the starting MOP, we attempted to synthesize variants of HRhMOP and OHRhMOP that would be soluble in aprotic organic solvents (*e.g.* dichloromethane and tetrahydrofuran) and in water. We did this by functionalizing the starting MOPs with either CF_3-Py (for its hydrophobicity) or L-Prol (for its hydrophilicity). For the former, we added CF_3-Py to a suspension of HRhMOP crystals in dichloromethane (DCM) or of OHRhMOP in tetrahydrofuran (THF) (Figure 2a). Instantaneously after addition of CF_3-Py, each suspension became a clear purple solution, giving rise to $[Rh_2(bdc)_2(CF3\text{-}Py)_1(H_2O)_1]_{12}$ and $[Rh_2(bdc\text{-}OH)_2(CF_3\text{-}Py)_1(H_2O)_1]_{12}$, respectively, as determined by UV-Vis and ^{1}H-NMR (Figure S7 to S10).

Similarly, we separately functionalized HRhMOP and OHRhMOP with L-Prol (again, 12 mol. eq.) by mixing each MOP with L-Prol in basic water (pH = 10.5). In both cases, we observed that upon addition of L-Prol, each suspension became a transparent purple solution, forming $[Rh_2(H\text{-}bdc)_2(L\text{-}prol)_1(H_2O)_1]_{12}$ and $[Rh_2(OH\text{-}bdc)_2(L\text{-}prol)_1(H_2O)_1]_{12}$ respectively, as confirmed by spectroscopic characterization (Figures S11 to S14)

Functionalization of MOPs with chiral amino acids is an alternative and straightforward strategy to confer them with chirality.[31] To this end, we functionalized HRhMOP and OHRhMOP with either L-Prol or D-Prol. The chirality of the resultant MOPs was studied by circular dichroism (CD) spectroscopy in solution. The enantiomeric MOPs exhibited opposite Cotton effects (Figures 2d and S15). Their CD spectra indicated a strong Cotton effect with the crossing wavelengths at 482 nm and 523 nm near the absorption of the Prol coordinated to the Rh-Rh paddle wheel unit in Rh-MOPs. The shape and magnitude of these Cotton effects clearly reflects the chiral coordination sphere of the Rh-Rh paddlewheel units in the MOPs. Thus, the sign of the CD signal is dictated by the enantiomeric form (L- or D-) of the proline.

At this point, we had demonstrated that the exterior axial sites of the Rh-Rh paddlewheel units serve as anchoring sites for N-donor ligands and that this reactivity can be used to introduce new functionalities and/or to selectively increase the solubility of Rh-MOPs in organic or aqueous media while preserving their intrinsic porosity (*vide infra*).

Post-synthetic functionalization via covalent chemistry

We next looked to a second source of reactive sites for post-synthetic functionalization of MOPs: their organic linkers. Cuboctahedral Rh(II)-based MOPs are assembled from 24 organic linkers. Accordingly, we considered that if each organic linker had one exohedral reactive functional group, then these MOPs could potentially be functionalized with 24 molecules (*i.e.* one per linker). We tested our hypothesis by functionalizing OHRhMOP through its 24 hydroxyl groups, using an acyl chloride and an acid anhydride under basic aqueous conditions.

The synthesis of esters from acyl chlorides and anhydrides entails nucleophilic attack to the carboxylic acid derivative by hydroxyl groups. To increase the nucleophilicity of the hydroxyl groups, these reactions are generally run in the presence of a strong base. Under these conditions, we observe that addition of NaOH (final pH = 10.5) to an aqueous suspension of OHRhMOP leads to dissolution of the MOP. This is due to deprotonation of the hydroxyl groups, which renders a negatively charged MOP, hereafter noted as *ONaRhMOP*. The integrity of ONaRhMOP was confirmed by UV-Vis, ^{1}H-NMR and mass spectrometry analysis in basic water, highlighting the high chemical stability of these MOPs (Figure S16 to S18).

We then exploited the solubility and nucleophilicity of ONaRhMOP to react it with acryloyl chloride (24 mol eq.; Figures 4a & 4b). For this, we performed a biphasic reaction by stirring an aqueous solution of ONaRhMOP and diethyl ether containing 1 mol. eq. of acryloyl chloride per phenolate group (*i.e.* 24 mol. eq. of acryloyl chloride per ONaRhMOP) overnight evolving from 0ºC to room temperature. The reaction product, which was precipitated at the interface after the overnight reaction, was washed with water and methanol and solubilized in DMF and analyzed by ^{1}H-NMR and mass spectrometry (Figures 4b, S19 and S20). Both techniques confirmed the quantitative conversion of the phenolate groups into the acrylate ester (hereafter named as *AcrRhMOP*). Indeed, the ^{1}H-NMR spectrum of AcrRhMOP evidenced generation of the acrylate ester, as indicated by the appearance of peaks at 6.52 ppm, 6.34 ppm and 6.14 ppm corresponding to the three protons of the acryloyl group.

The conversion rate was calculated by comparing the integration of the acrylate signals to the integration of the peak at 7.72 ppm, which corresponds to the outer aromatic proton of the OH-bdc ligand. As expected, the molar ratio of acrylate esters per Rh(II)-based MOP was 24:1. In addition, further evidence of the quantitative functionalization with acrylate esters was acquired by matrix-assisted laser desorption/ionization-time of flight (MALDI-TOF), which showed a peak at *m/z* = 8090.5 that matches the molecular formula of the protonated desired fully-functionalized Rh-MOP, $[Rh_2(Acr\text{-}bdc)_2 + H^+]^+$ (*m/z* = 8090.9).

To further evaluate the reactivity of the phenolate groups in ONaRhMOP, we reacted it with acetic anhydride in conditions analogous to those for acryloyl chloride. The reaction solid was washed once with methanol, dissolved in DMF, and then, analyzed by ^{1}H-NMR and mass spectrometry (Figures 4c, S22 and S23). In this case, both techniques showed the partial functionalization of the Rh-MOP with acetate ester groups (hereafter named as *OMetRhMOP*). The esterification was confirmed by the ^{1}H-NMR spectrum, which showed a new peak at 2.25 ppm, corresponding to the methyl group. The relative intensity of the integrations of the peak at 2.25 ppm and the outer proton of the OH-bdc was used to estimate that the conversion rate was *ca.* 75%, meaning that 18 of the available 24 phenolates had been converted to esters. This result was confirmed by MALDI-TOF, which showed a peak at *m/z* = 7968.9, consistent with a partially functionalized Rh-MOP of formula $[Rh_{24}(OH\text{-}bdc)_6(OMet\text{-}bdc)_{18} + H]^+$ + DCTB + DMF + MeOH (*m/z* = 7969.9). Subsequent reactions using more acetic anhydride did not provide any improvement in conversion, suggesting that, under the tested conditions, full conversion of the phenolate groups was precluded due to steric hindrance between the derivatized OMetRhMOP and the acetic anhydride.

Post-synthetic dual functionalization via combined coordination and covalent chemistries

We next explored the possibility of functionalizing OHRhMOP at its two types of reactive sites (the axial site of the Rh-Rh paddlewheel units and the hydroxyl groups of the organic linkers) using coordination chemistry for the former and covalent chemistry for the latter, reasoning that these two approaches should not be mutually exclusive. We envisaged that combining these chemistries would enable us to functionalize the external surface of these MOPs with a total of 36 functional groups. We demonstrated this by functionalizing AcrRhMOP with 12 tertPy molecules. Addition of tertPy (12 mol eq.) to a DMF solution of AcrRhMOP caused the solution to immediately change color from green to purple. The expected product was then confirmed by UV-VIS and ^{1}H-NMR as for the previous products (Figures S25 and S26).

Once we had confirmed the dual functionalization of OHRhMOP with 12 tertPy ligands and 24 esters, we investigated the use of the same two chemistries for functionalizing OHRhMOP by formation of ether linkages. Interestingly, although esters could be

prepared from acyl chlorides or anhydrides at room temperature due to the high reactivity of both functional groups, ethers could not be prepared from halogenated compounds under similar reaction conditions. This result is not surprising, as the standard conditions to alkylate a hydroxyl group with brominated alkanes entails use of high boiling-point solvents (*e.g.* DMF) and high temperatures (*i.e.* above 80 °C) in the presence of an inorganic base. However, OHRhMOP is not soluble in DMF, which implies that any reaction in this solvent should be carried out under heterogeneous conditions. Unfortunately, the heterogeneous reaction between OHRhMOP and allyl bromide in DMF at 80 °C failed. We reasoned that the close packing of OHRhMOP in the solid state hindered the diffusion of the reagents, thereby preventing conversion of the hydroxyl groups.

To overcome this low solubility, we employed dual functionalization to first dissolve the OHRhMOP in DMF by coordinating tertPy (*vide supra*). Then, the functionalized OHRhMOP (tertPy) was reacted *in situ* with allyl bromide (Figure 5a). This sequential functionalization was carried out by simply mixing the three components in DMF, and the resulting purple solution was stirred at 80ºC for 12 hours. After this period, the MOP was precipitated by diethyl ether, washed with methanol and acetone and dried under ambient conditions.

UV-Vis and ^{1}H-NMR analyses of the purified product dissolved in DMF confirmed that both types of conversion had occurred. Indeed, the UV-VIS spectrum showed the characteristic λ_{max} of 555 nm (Figure 5c). In addition, the ^{1}H-NMR spectrum showed the presence of peaks corresponding to tertPy (9.48 ppm and 8.55 ppm for the aromatic protons, and 1.36 ppm for the tert-butyl group) and to the allyl group (5.91 ppm, 5.30 ppm, 5.17 ppm and 4.46 ppm). The relative integration between the allyl protons and the aromatic protons of the OH-bdc ligand revealed a conversion degree of 40%. The doubly-functionalized Rh-MOP product is referred to hereafter as *Oallyl RhMOP(tertPy)* (Figures 5b and S27).

Interestingly, the reversible nature of the coordination bond between the Rh-Rh paddlewheel and the tertPy ligands enabled us to selectively cleave them after the covalent reaction, leading to their replacement with water. Under aqueous conditions, this cleavage and ligand exchange occur at a pH below 2.1. Thus, this cleavage was performed by adding one drop of 3M HCl to a suspension of OallylRhMOP(tertPy) in acetone or water, inducing a sudden color shift in the suspension, from purple to green. This color change was an indication of the ligand-exchange between the tertPy and H_2O ligands, which was further corroborated by the UV-Vis spectrum, through the expected shift in λ_{max}, from 555 nm to 590 (Figure 5c). Moreover, the ^{1}H-NMR spectrum of the acid-treated MOP confirmed that all the tertPy ligands had been cleaved while the integrity of the allyl functionality was preserved, which yielded a new product referred to hereafter as *OAllyl RhMOP (*Figure 5b). MALDI-TOF of Rh-OAllyl-MOP confirmed its functionalization with allyl groups, showing a peak at *m/z* =7419.4, which corresponds to the following formula: $[Rh_{24}(OH\text{-}bdc)_{15}(OAllyl\text{-}bdc)_9 + H]^+ + DCTB + H_2O$ (*m/z* = 7418.3) (Figure S28).

Porosity of functionalized Rh-MOPs

Finally, to confirm that functionalized Rh-MOPs maintain their porous character in the solid state, we submitted all these materials to N_2 sorption tests at 77 K (Figure S29-S40). All amorphous functionalized Rh-MOPs showed a type I adsorption isotherm, indicating that the inner microporous cavity was preserved despite the post-synthetic modifications. However, as expected,[32,33] we found that the outer functionalization in all Rh-MOPs induced a decrease in their S_{BET} as compared to the parent materials, HRhMOP and OHRhMOP, which showed the highest BET surface areas (S_{BET}), with values of 947 m^2/g and 548 m^2/g, respectively. Functionalized HRhMOPs showed lower S_{BET} values: 675 m^2/g for HRhMOP(CF_3-Py), 589 m^2/g for HRhMOP(tertPy) and 337 m^2/g for HRhMOP (L-Prol). In the case of functionalized OHRhMOPs, a similar trend was observed: 154 m^2/g for OHRhMOPs (CF_3-Py), 388 m^2/g for OHRhMOPs(tertPy), and 64 m^2/g for OHRhMOPs(L-Prol), respectively. Finally, the covalently functionalized Rh-MOPs exhibited an S_{BET} of 410 m^2/g for AcrRhMOP, 120 m^2/g for AcrRhMOP(tertPy), 487 m^2/g for OMetRhMOP. OallylRhMOP was found to be non-porous to N_2 but porous to CO_2 reaching a maximum uptake of 1.15 mmol/g at 1 bar and 298k. Altogether, these results confirm that, despite the conditions to which functionalized Rh-MOPs were exposed, they retained their intrinsic microporosity in the solid state.

CONCLUSIONS

In conclusion, we have demonstrated post-synthetic functionalization of Rh-based MOPs via two chemistries at two types of reactive sites: coordination chemistry at their Rh-Rh paddlewheel units, and covalent chemistry at their organic linkers. Functionalization of the 12 Rh-Rh paddlewheel units was demonstrated by coordinating N-donor ligands, whose relative hydrophobicity dictated the solubility of the resultant products. This coordination approach was also used to confer Rh-MOPs with chirality. Through covalent chemistry, the 24 hydroxyl groups on the organic linkers were converted into esters by reacting them with acyl chlorides or acid anhydrides. The orthogonal reactivity of the Rh-Rh paddlewheel units and the organic linkers enabled us to combine the two chemistries to yield doubly-functionalized Rh-MOPs featuring a total of 36 new functional molecules. We believe that the stoichiometrically and spatially controlled functionalization of MOPs can provide structurally well-defined nanoscopic platforms for delivery, sorption and catalytic applications.

EXPERIMENTAL SECTION

Materials and Instruments

Rhodium acetate, 1,3-benzenedicarboxylic acid, 5-hydroxy-1,3-benzenedicarboxylic acid, acryloyl chloride, acetic anhydride and allyl bromide were purchased from Sigma Aldrich and used as received. Solvents at HPLC grade were purchased from Fischer chemicals.

Powder X-Ray Diffraction (PXRD) patterns were recorded on an X'Pert PRO MPD analytical diffractometer (Panalytical) at 45 kV, 40 mA using CuKα radiation (λ = 1.5419 Å). Nitrogen gas-sorption isotherms were measured at 77K and at 298K using an Autosorb-IQ-AG analyzer. UV-Vis was measured in an Agilent Cary 4000 and circular dichroism was measured in a J-715 CD spectrophotometer (JASCO), both at room temperature (*ca.* 25 °C). ^{1}H NMR spectra were acquired in Bruker Avance III 400SB NMR spectrometer. Mass spectrometry (MALDI-TOF) was run in an Applied Biosystems 4700 Proteomics Analyzer operating in positive-ionization mode.

Synthesis of Rh-MOPs

HRhMOP. 100 mg of $Rh_2(acetate)_4{\cdot}2MeOH$ (0.2 mmol), 160 mg of isophthalic acid (0.96 mmol), and 105 mg of Na_2CO_3 (1 mmol) were dispersed in 7 mL of DMA. The mixture was transferred to a scintillation vial and heated at 100 °C for 48 h. A microcrystalline powder was separated from the reaction mixture and washed with DMA, EtOH and MeOH. Finally, microcrystals were kept in acetone overnight and dried at 85 °C under vacuum. Single crystals of Rh-H-MOP were prepared by heating a dispersion of 10 mg of $Rh_2(acetate)_4{\cdot}2MeOH$ (0.02 mmol), 10 mg of 1,3-benzenedicarboxylic acid (0.06 mmol) and 1.5 mg of K2CO3 (0.01 mmol) in 1 mL of DMA in a scintillation vial at 100 °C for 48 h.

OHRhMOP. 100 mg of $Rh_2(acetate)_4{\cdot}2MeOH$ (0.2 mmols), 180 mg of 5-hydroxy-1,3-benzenedicarboxylic acid (0.96 mmols) and 105 mg of Na_2CO_3 (1 mmol) were dispersed in 7 mL of DMA. The mixture was transferred to a scintillation vial and heated at 100 °C for 48 h. The resulting OHRhMOP single crystals were washed with DMA and dissolved in MeOH to separate them from Na_2CO_3. The solution was dried under vacuum, and the residue washed with water and acetone. Finally, the powder was kept in acetone overnight and dried at 85 °C under vacuum.

HRhMOP (tertPy). 17 μL of tertPy (111 μmol) were added to a dispersion of 60 mg of HRhMOP (9.3 μmol) in 10 mL of DMF. The resulting mixture was sonicated for 5 min and then, centrifuged at 18000 rpm for 10 min. The supernatant was collected and precipitated with ether vapors over 5 days to yield single purple crystals. HRhMOP(tertPy) crystals were then separated from the mother liquor and washed with ether and acetone. Finally, the sample was kept in acetone overnight and dried at 85 °C under vacuum. Note that OHRhMOP*(tertPy)* was prepared using the same conditions as for HRhMOP*(tertPy)*, except that instead of 17 μL of tertPy, 15 μL were used.

HRhMOP (CF_3-Py). 13 μL of CF_3-Py (111 μmol) were added to a dispersion of 60 mg of HRhMOP(9.3 μmol) in 10 mL of dichloromethane. This mixture was sonicated for 5 min. Then, it was filtered and the filtrate was evaporated under vacuum. The resulting solid was washed with acetone. Finally, the sample was kept in acetone overnight and dried at 85ºC under vacuum. Note here that OHRhMOP(CF_3-Py) was prepared using the same conditions as for HRhMOP(tertPy), except that instead of using 13 μL of tertPy and dichloromethane as solvent, 12 μL of tertPy were used and THF was the solvent.

HRhMOP(L-Prol). A solution of 13 mg of L-Prol (111 μmol) in 1 mL of water at a pH = 10.5 (pH was adjusted with NaOH) was added to a dispersion of 60 mg of HRhMOP (9.3 μmol) in 5 mL of water. The resulting mixture was sonicated for 5 min and the solution was centrifuged at 18000 rpm for 10 min. The supernatant was collected and precipitated with acetone vapors over 10 days to yield purple crystals. HRhMOP(L-Prol) crystals were separated from the mother liquors and washed with acetone. Finally, the sample was kept in acetone overnight and dried at 85 °C under vacuum. Note here that HRhMOP(D-Prol) was prepared using the same conditions as for HRhMOP(L-Prol), except that instead of L-Prol, we used D-Prol. The same protocol was also used to obtain OHRhMOP(L-Prol) and OHRhMOP(D-Prol).

AcrRhMOP. 4.3 mg (105 μmol) of NaOH were added to a dispersion of 30 mg of OHRhMOP (4.4 μmol) in 1 mL of water. After this addition, the OHRhMOP dissolved instantly, due to deprotonation of the phenol groups. Then, a diethyl ether solution containing 8.5 μL of acryloyl chloride (105 μmol) was layered on top of the as-made ONaRhMOP aqueous solution at 0 °C. The biphasic mixture was vigorously stirred overnight at room temperature. Afterwards, a green solid appeared at the interphase; it was isolated, and then washed with MeOH and acetone. Finally, the sample was kept in acetone overnight and dried at 85 °C under vacuum. Note here that OMetRhMOP was prepared using the same conditions as for AcrRhMOP, except that instead of using 8.5 μL of acryloyl chloride and diethyl ether as solvent, 15 μL of acetic anhydride (137 μmol) were used and 1,4-dioxane was the solvent.

AcrRhMOP(tertPy). 10 mg of AcrRhMOP (1.2 μmol) were dissolved 5 mL of DMF. Then, 100 μL of a 1 mL stock solution of tertPy containing 18 μL (120 μmol) were added to the Rh-Acr-MOP solution, causing an immediate color change from green to purple. AcrRhMOP(tertPy) was precipitated by adding diethyl ether. The solid was washed with ether and dried under vacuum.

OAllylRhMOP(tertPy). 30 mg of OHRhMOP (4.4 μmol) were dissolved in 2 mL of DMF by adding 10 μL of tertPy (66 μmol). Then, 45 mg of K_2CO_3 (316 μmol) were added to the Rh-OH-MOP(tertPy) solution. The mixture was stirred at 80 °C for 30 min. Then, 14 μL of allyl bromide (316 μmol) were added, and the resulting mixture was reacted at 80 °C for 24 h. The final purple-reddish solution was centrifuged, and the supernatant evaporated under vacuum to obtain a purple residue. The crude product was washed with diethyl ether, MeOH and acetone, and dried at 85 °C under vacuum.

OAllylRhMOP. 100 μL of 3M HCl was added to a dispersion of 20 mg of OAllylRhMOP(tertPy) in acetone at room temperature. The purple suspension rapidly became green, indicating decoordination of tertPy. The solid was recovered by centrifugation and further washed with water and MeOH. Finally, the sample was kept in acetone overnight and dried at 85 °C under vacuum.

ASSOCIATED CONTENT

The Supporting Information is available free of charge via the Internet at http://pubs.acs.org.

Single-crystal X-ray diffraction of HRhMOP(CCDC 1883914), OHRhMOP (CCDC 1883124) and HRhMOP(tertPy) (CCDC 1884202), XRPD, ^{1}H-NMR, UV-Vis, MALDI-TOF and sorption data.

AUTHOR INFORMATION

Corresponding Author

* arnau.carne@icn2.cat
* shuhei.furukawa@icems.kyoto-u.ac.jp
* daniel.maspoch@icn2.cat

Orcid

Arnau Carné Sánchez 0000-0002-8569-6208
Inhar Imaz 0000-0002-0278-1141
Shuhei Furukawa 0000-0003-3849-8038
Daniel Maspoch 0000-0003-1325-9161

Notes

The authors declare no competing financial interest.

Author Contributions

#ACS, JA and TG contributed equally

ACKNOWLEDGMENT

The authors thank to Ms. Nao Horike, Dr. Mio Kondo, Dr. Nicolas Louvain and Dr. Gavin Craig for their preliminary works on the synthesis of OH-RhMOP. This work was supported by the Spanish MINECO (projects PN MAT2015-65354-C2-1-R), the Catalan AGAUR (project 2014 SGR 80), and the ERC under the EU-FP7 (ERC-Co 615954). It was also funded by the CERCA Program/Generalitat de Catalunya. ICN2 is supported by the Severo Ochoa program from the Spanish MINECO (Grant No. SEV-2017-0706). A.C.S. and T.G. thank the Spanish MINECO for Juan de la Cierva fellowship (IJCI-2016-29802 and FJCI-2017-31598). J.A acknowledges the Generalitat de Catalunya for an FI fellowship. This study was supported by JSPS KAKENHI Grand Number 18H01995 (Kiban B) and 17H05367 (Coordination Asymmetry). iCeMS is supported by the World Premier International Research Initiative (WPI), MEXT, Japan.

REFERENCES

(1) Jin, R.; Zeng, C.; Zhou, M.; Chen, Y. Atomically Precise Colloidal Metal Nanoclusters and Nanoparticles: Fundamentals and Opportunities. *Chem. Rev.* **2016**, 116, 10346.

(2) Gargas, D. J.; Chan, E. M.; Ostrowski, A. D.; Aloni, S.; Altoe, M. V. P.; Barnard, E. S.; Sanii, B.; Urban, J. J.; Milliron, D. J.; Cohen, B. E.; Schuck, P. J. Engineering bright sub-10-nm upconverting nanocrystals for single-molecule imaging. *Nat. Nanotech.* **2014**, 9, 300.

(3) Kim, B. H.; Hackett, M. J.; Park, J.; Hyeon, T. Characterization, and Application of Ultra-small Nanoparticles. *Chem. Mater.***2014**, 26, 59.

(4) Liu, Q.; Sun, Y.; Yang, T.; Feng, W.; Li, C.; Li, F. Sub-10 nm Hexagonal Lanthanide-Doped NaLuF4 Upconversion Nanocrystals for Sensitive Bioimaging in Vivo. *J. Am Chem Soc*. **2011**, 133, 17122.

(5) Ma, K.; Sai, H.; Wiesner, U. Ultra-small Sub-10 nm Near-Infrared Fluorescent Mesoporous Silica Nanoparticles. J. *Am. Chem. Soc.* **2012**, 134, 13180.

(6) Zarschler, K.; Rocks, L.; Licciardello, N.; Boselli, L.; Polo, E.; Garcia, K. P.; De Cola, L.; Stephan, H.; Dawson, K. A. Ultra-small inorganic nanoparticles: State-of-the-art and perspectives for biomedical applications. *Nanomedicine: NBM*, **2016**, 12, 1663.

(7) Tranchemontagne, D. J.; Ni, Z.; O'Keeffe, M.; Yaghi, O. M. Reticular Chemistry of Metal–Organic Polyhedra. *Angew. Chem. Int. Ed.* **2008**, 47, 5136.

(8) Cullen, W.; Misuraca, M. C.; Hunter, C. A.; Williams, N. H.; Ward, M. D. Highly efficient catalysis of the Kemp elimination in the cavity of a cubic coordination cage. *Nat. Chem.* **2016**, 8, 231.

(9) Fujita, D.; Ueda, Y.; Sato, S.; Mizuno, N.; Kumasaka, T.; Fujita, M. Self-assembly of tetravalent Goldberg polyhedra from 144 small components. *Nature* **2016**, 540, 563.

(10) Zhang, D.; Ronson, T. K.; Nitschke, J. R. Functional Capsules via Subcomponent Self-Assembly. *Acc. Chem. Res.* **2018**, 51, 2423.

(11) Cook, T. R.; Stang, P. J. Recent Developments in the Preparation and Chemistry of Metallacycles and Metallacages via Coordination. *Chem. Rev.* **2015**, 115, 7001.

(12) Li, J.-R.; Zhou, H.-C. Bridging-ligand-substitution strategy for the preparation of metal–organic polyhedra. *Nat. Chem.* **2010**, 2, 893.

(13) Rowland, C. A.; Lorzing, G. R.; Gosselin, E. J.; Trump, B. A.; Yap, G. P. A.; Brown, C. M.; Bloch, E. D. Methane Storage in Paddlewheel-Based Porous Coordination Cages. *J. Am. Chem. Soc.* **2018**, 140, 11153.

(14) Liu, G.; Ju, Z.; Yuan, D.; Hong, M. In Situ Construction of a Coordination Zirconocene Tetrahedron. *Inorg. Chem.* **2013**, 52, 13815.

(15) Li, J-R.; Yu, J.; Lu, W.; Sun, L-B.; Sculley, J.; Balbuena, P.; Zhou, H-C. Porous materials with pre-designed single-molecule traps for CO2 selective adsorption. *Nat. Commun.* **2013**, 4, 1583.

(16) Xing, W-H.; Li, H-Y.; Dong, X-Y.; Zang, S-Q. Robust multifunctional Zr-based metal–organic polyhedra for high proton conductivity and selective CO2 capture. *J. Mater. Chem. A.* **2018**, 6, 7724.

(17) (a) Eddaoudi, M.; Kim, J.; Wachter, J. B.; Chae, H. K.; O'Keeffe, M.; Yaghi, O. M. Porous Metal−Organic Polyhedra: 25 Å Cuboctahedron Constructed from 12 Cu2(CO2)4 Paddle-Wheel Building Blocks. *J. Am. Chem. Soc.* **2001**, 123, 4368. (b) Park, J.; Perry, Z.; Chen, Y-P.; Bae, J.; Zhou, H-C. Chromium(II) Metal−Organic Polyhedra as Highly Porous Materials. *ACS Appl. Mater. Interfaces.* **2017**, 9, 28064. (c) Ke, Y.; Collins, D. J; Zhou, H-C. Synthesis and Structure of Cuboctahedral and Anticuboctahedral Cages Containing 12 Quadruply Bonded Dimolybdenum Units. *Inorg. Chem.* **2005**, 44, 4154. (d) Furukawa, S.; Horike, N.; Kondo, M.; Hijikata, Y.; Carné-Sánchez, A.; Larpent, P.; Louvain, N.; Diring, S.; Sato, H.; Matsuda, R.; Kawano, R.; Kitagawa, S. Rhodium–Organic Cuboctahedra as Porous Solids with Strong Binding Sites. *Inorg. Chem.* **2016**, 55, 10843. (e) Young, M. D.; Zhang, Q.; Zhou, H-C. Metal–organic polyhedra constructed from dinuclear ruthenium paddlewheels. *Inorganica Chim. Acta.* **2015**, 424, 216. (f) Teo, J. M.; Coghlan, C. J.; Evans, J. D.; Tsivion, E.; Head-Gordon, M.; Sumby, C. J.; Doonan, C. J. Hetero-bimetallic metal–organic polyhedra. *Chem. Commun.* **2016**, 52, 276.

(18) Boselli, L.; Polo, E.; Castagnola, V.; Dawson, K. A. Regimes of Biomolecular Ultra-small Nanoparticle Interactions. *Angew. Chem. Int. Ed.* **2017**, 56, 4215.

(19) Jiang, Y.; Huo, S.; Mizuhara, T.; Das, R.; Lee, Y.-W.; Hou, S.; Moyano, D. F.; Duncan, B.; Liang, X.-J.; Rotello, V. M. The Interplay of Size and Surface Functionality on the Cellular Uptake of Sub-10 nm Gold Nanoparticles. *ACS Nano* **2015**, 9, 9986.

(20) Kim, B. H.; Hackett, M. J.; Park, J.; Hyeon, T. Synthesis, Characterization, and Application of Ultrasmall Nanoparticles. *Chem. Mater.* **2014**, 26, 59.

Table of Contents

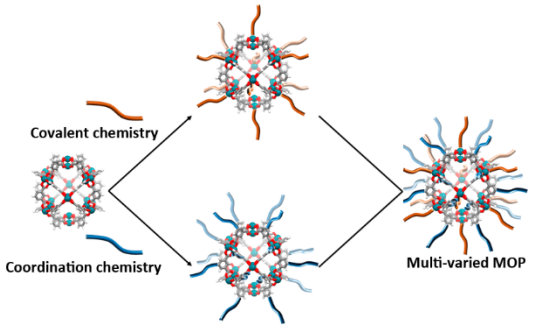

FIGURES

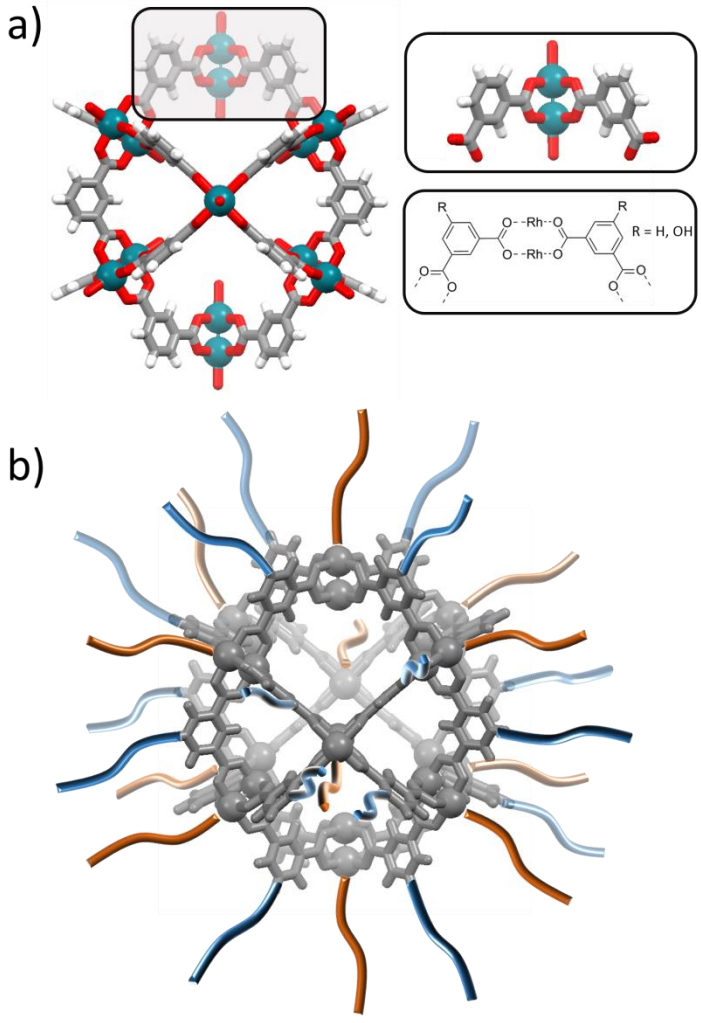

Figure 1. (a) Structure of a cuboctahedron Rh-MOP, highlighting the coordination and composition of the Rh-Rh paddlewheel units. Color key: green: rhodium; red: oxygen; grey: carbon; white: hydrogen. (b) Illustration of a cuboctahedron Rh-MOP functionalized on the 12 dirhodium paddlewheels through coordination chemistry (in orange) and on the 24 organic linkers through covalent chemistry (in blue).

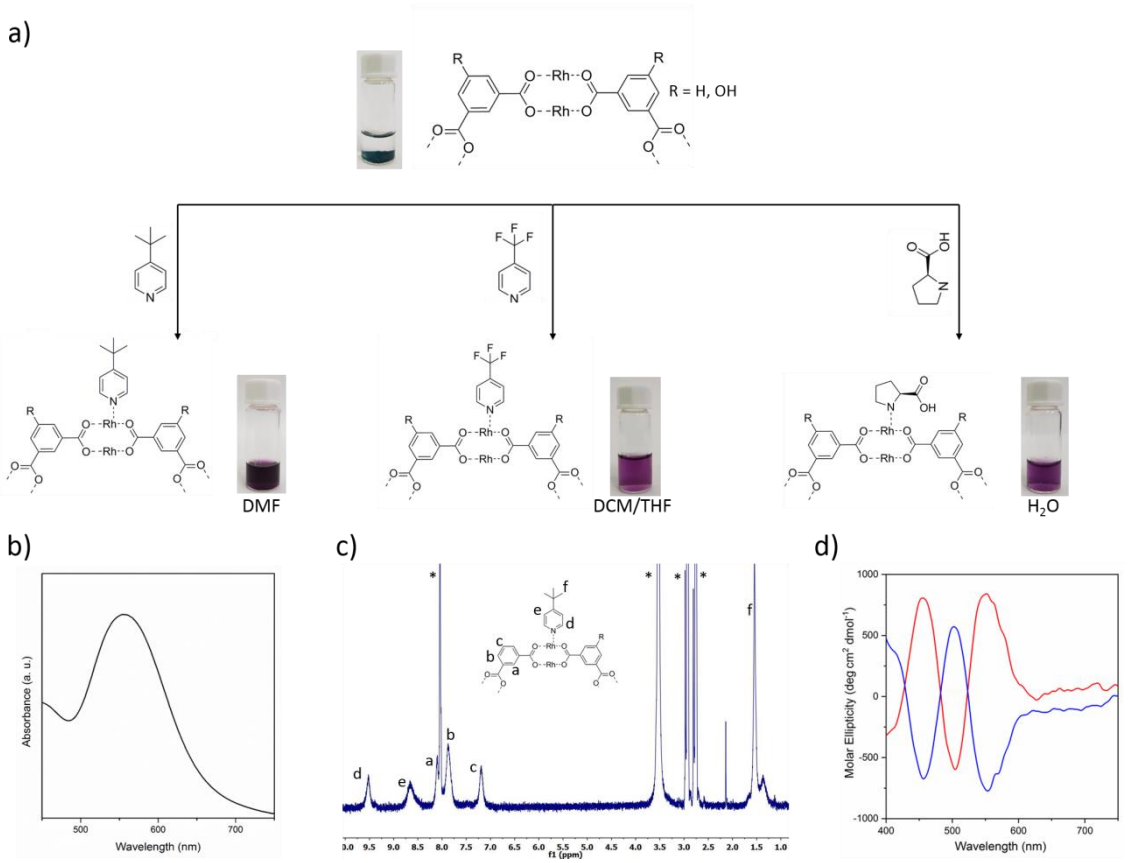

Figure 2. (a) Schematic representation showing the post-synthetic modification of HRhMOP and of OHRhMOP via coordination of N-based ligands at the corresponding dirhodium axial sites. The photographs illustrate the initial dispersion of insoluble HRhMOP or OHRhMOP in DMF, DCM, THF or H2O (top), and the purple solutions resulting from post-synthetic functionalization reactions with tertPy (left), CF3-Py (center) or L-Prol (right). (b) UV-Vis spectrum of HRhMOP (tertPy) in DMF showing a λ_{max} at 555 nm. (c) ^{1}H-NMR of HRhMOP (tertPy) in DMF-d_7. Solvent peaks (DMF and water) are labeled with an asterisk. (d) CD spectra of HRhMOP (L-Prol) (red) and HRhMOP (D-Prol) (blue) in water.

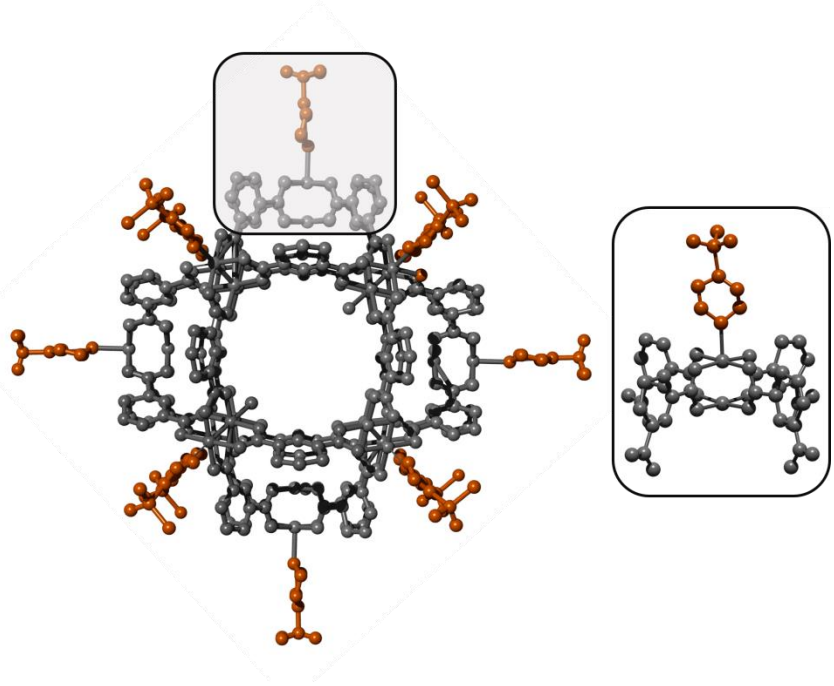

Figure 3. Crystalline structure of HRhMOP(tertPy). The coordination of tertPy to the Rh-Rh axial site is highlighted.

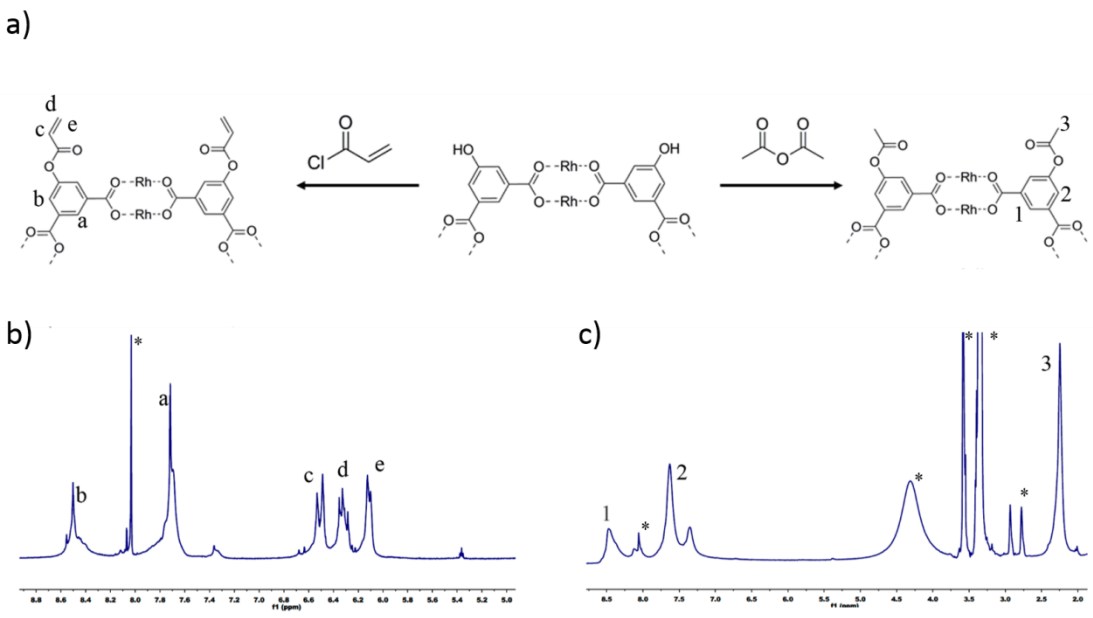

Figure 4. (a) Schematic showing the covalent post-synthetic functionalization of OHRhMOP via formation of ester linkages. (b) 1H-NMR of AcrRhMOP in DMF-d7. (c) 1H-NMR of OMetRhMOP in DMF-d_7. Solvent peaks [DMF in (b) and DMF, MeOH, dioxane and water in (c)] are highlighted with an asterisk

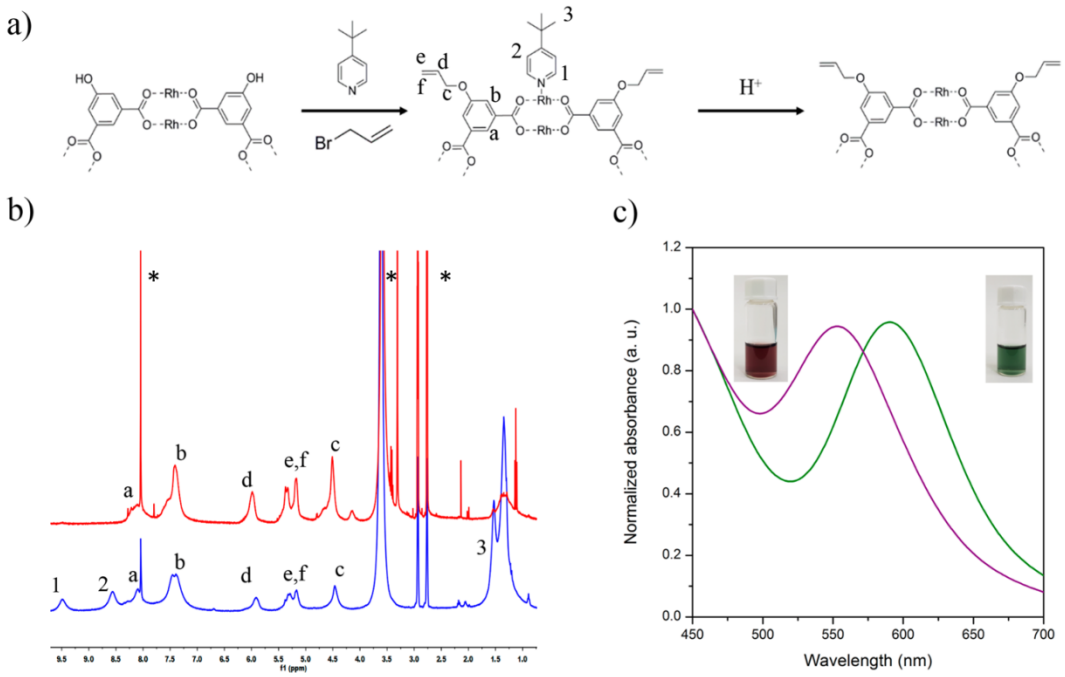

Figure 5. (a) Schematic showing the sequential coordination-covalent functionalization of OHRhMOP with ether linkages. (b) 1H-NMR of OallylRhMOP(tertPy) (blue) and OallylRhMOP (red) in DMF-d7. Solvent peaks (DMF and water) are highlighted with an asterisk. (c) UV-Vis spectra of OallylRhMOP (tertPy) (purple) and OallylRhMOP (green) in DMF, showing the shift of λmax from 555 nm to 590 nm. Inset: photographs of each solution.